

Electronic Supplementary Information

for

Chirality meets visible-light photocatalysis in a molecular cerium vanadium oxide cluster

Andrey Seliverstov, Carsten Streb

Institute of Inorganic Chemistry I, Ulm University, Albert-Einstein-Allee 11, 89081 Ulm, Germany

carsten.streb@uni-ulm.de

Table of Contents

S1.	Analytical methods and instrumentation	1
S2.	Synthetic section	2
S3.	Single crystal x-ray diffraction	3
S4.	Cryospray ionization mass-spectroscopy.....	6
S5.	Thermogravimetric analysis.....	7
S6.	UV-Vis-NIR spectroscopy.....	7
S7.	Photooxidative activity	8
S8.	Bibliography	12

S1. Analytical methods and instrumentation

X-ray diffraction. Single-crystal X-ray diffraction studies were performed on a Nonius Kappa CCD Single-crystal X-ray diffractometer equipped with a graphite monochromator using MoK α radiation ($\lambda(\text{MoK}\alpha) = 0.71073 \text{ \AA}$).

UV-Vis-NIR spectroscopy. UV-Vis spectroscopy was performed on a *Shimadzu* UV-3600 UV-Vis-NIR spectrophotometer with standard cuvettes ($d = 10.0 \text{ mm}$).

Thermogravimetry analysis (TGA). TGA was performed on a *Setaram Setsys CS Evo*, 30 – 700 °C @10K/min, He atmosphere, quartz crucible 0.5 mL.

FT-IR spectroscopy. FT-IR spectroscopy was performed on a *Shimadzu FT-IR 8400* spectrometer. Signals are given as wavenumbers in cm^{-1} using the following abbreviations: *vs* – very strong, *s* – strong, *m* – medium, *w* – weak and *b* – broad.

Elemental analysis. CHN-analysis was performed on a *Euro Vector Euro EA 3000 Elemental Analyzer*. Ce and V were analyzed with inductively coupled plasma atomic emission spectroscopy (ICP-AES) analyses on *SPECTRO CIROS-CCP* spectrometer.

ESI Mass spectrometry (ESI-MS). MS measurements were performed on a UHR-ToF *Bruker Daltonik* (Bremen, Germany) *maXis*, which was coupled to a *Bruker* cryospray unit, an ESI-ToF MS capable of resolution of at least 40.000 FWHM. Detection was in negative-ion mode and the source voltage was 4.5 kV. The flow rates were 300 $\mu\text{L/h}$. The drying gas (N_2), was held at $-55\text{ }^\circ\text{C}$ and the spray gas was held at $-60\text{ }^\circ\text{C}$. The machine was calibrated prior to every experiment via direct infusion of the *Agilent* ESI-TOF low concentration tuning mixture, which provided an m/z range of singly charged peaks up to 2700 Da in both ion modes. Concentration was ca. 1×10^{-4} M.

General remarks. All chemicals were purchased from *Sigma Aldrich* or *ABCR* and were of reagent grade. $(n\text{Bu}_4\text{N})_3[\text{H}_3\text{V}_{10}\text{O}_{28}]$ and $(n\text{Bu}_4\text{N})_4[\text{V}_4\text{O}_{12}]$ were prepared according to published procedures.^{S1,2} The chemicals were used without further purification unless stated otherwise.

S2. Synthetic section

Compound 1, $(n\text{Bu}_4\text{N})_2[(\text{Ce}(\text{dmsO})_3)_2\text{V}_{12}\text{O}_{33}\text{Cl}] \times 2\text{DMSO}$. $(n\text{Bu}_4\text{N})_3[\text{H}_3\text{V}_{10}\text{O}_{28}]$ (1500 mg, 0.96 mmol, 1 eq) and cerium(III) chloride heptahydrate (662 mg, 1.78 mmol, 1.85 eq) are dissolved in 22 mL of DMSO under vigorous stirring and heated to $80\text{ }^\circ\text{C}$ for 2 h. Subsequently, addition of 2.50 mL of 1.5M aqueous $n\text{Bu}_4\text{NOH}$ leads to a dark-brown solution. Vapor diffusion crystallization (acetone as the diffusion solvent) of this solution gives brown crystals of the target product after 4 weeks. Yield: 0.456 g, 0.18 mmol, 25% (based on V). Drying in desiccator leads to the loss of 1 DMSO molecule. Elemental analysis for $\text{C}_{46}\text{H}_{114}\text{Ce}_2\text{ClN}_2\text{O}_{40}\text{S}_7\text{V}_{12}$ in wt.-% (calcd.): C 22.15 (22.22), H 4.62 (4.62), N 1.10 (1.13), S 8.74 (9.03), V 23.71 (23.83), Ce 10.31 (10.93). Characteristic IR bands (in cm^{-1}): 3443(m,b), 2929(w,b), 2880(w,b), 2365(m), 1672(s), 1640(s,b), 1510(m), 1410(m), 1308(m), 1260(w), 1223(w), 1115(w), 995(s), 826(m,b), 764(m), 644(s,b), 557(m), 517(w), 465(w).

S3. Single crystal x-ray diffraction

Table S1. Crystallographic data for compound **1**

CCDC reference no	959107
Empirical formula	C ₄₈ H ₁₂₀ Ce ₂ ClN ₂ O ₄₁ S ₈ V ₁₂
Formula weight	2564.90
Temperature / K	150(2)
Crystal system	monoclinic
Space group	<i>C2/c</i>
<i>a</i> / Å	18.593(4)
<i>b</i> / Å	23.844(5)
<i>c</i> / Å	20.988(4)
α / °	90
β / °	95.24(3)
γ / °	90
Volume / Å ³	9266(3)
<i>Z</i>	4
ρ_{calc} / mg/mm ³	1.839
μ / mm ⁻¹	2.397
<i>F</i> (000)	5148.0
Crystal size / mm ³	0.25 × 0.18 × 0.09
2 θ range for data collection	5.572 to 53.002°
Index ranges	-23 ≤ <i>h</i> ≤ 23, -29 ≤ <i>k</i> ≤ 29, -25 ≤ <i>l</i> ≤ 26
Reflections collected	74694
Independent reflections	9600 [<i>R</i> _{int} = 0.0373]
Data/restraints/parameters	9600/354/534
Goodness-of-fit on <i>F</i> ²	1.068
Final <i>R</i> indexes [<i>I</i> ≥ 2 σ (<i>I</i>)]	<i>R</i> ₁ = 0.0267, <i>wR</i> ₂ = 0.0715
Final <i>R</i> indexes [all data]	<i>R</i> ₁ = 0.0368, <i>wR</i> ₂ = 0.0758
Largest diff. peak/hole / e Å ⁻³	1.32/-1.58

Crystals are stable in air under ambient conditions and are not hygroscopic. Structure solution and refinement were carried out with *SHELXS-2013/2* and *SHELXL-2013/2*^{S3} via *OLEX2*^{S4}. Most of the non-hydrogen atoms were refined anisotropically. Hydrogen atoms were added using a riding model. Absorption correction was applied via *SADABS 2.03*. *Platon*^{S5} (*TwinRotMat*) and *OLEX2* scripts for twin law search were used to exclude possible twinning. The geometry and anisotropic refinement of the solvent and ligand molecules was restrained using *SADI*, *SIMU* and *DELU*. The metal oxo frameworks of all clusters were refined fully anisotropically and no restraints were used.

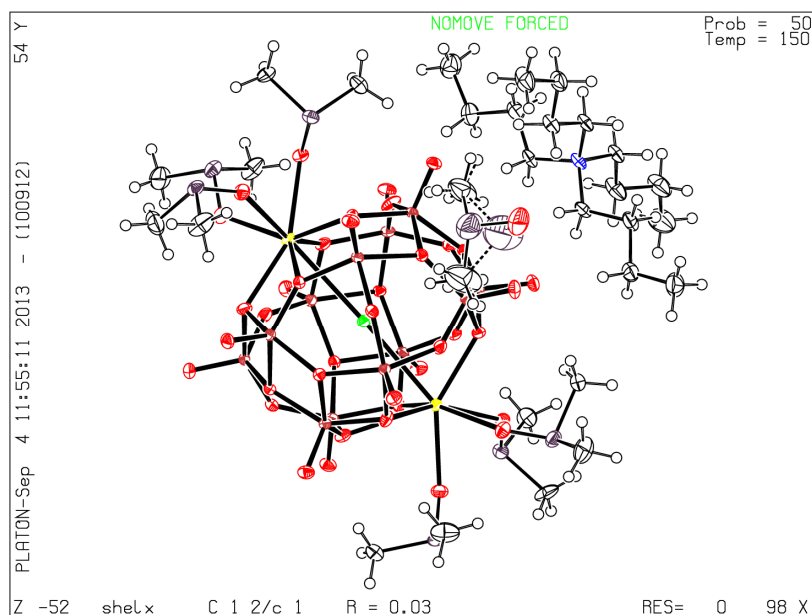


Figure S1. ORTEP diagram for **1**. Thermal ellipsoids are shown at 50% probability. Color scheme: Ce: yellow; V: vermilion; O: maroon; S: purple; Cl: neon-green; N: blue; C, H: black

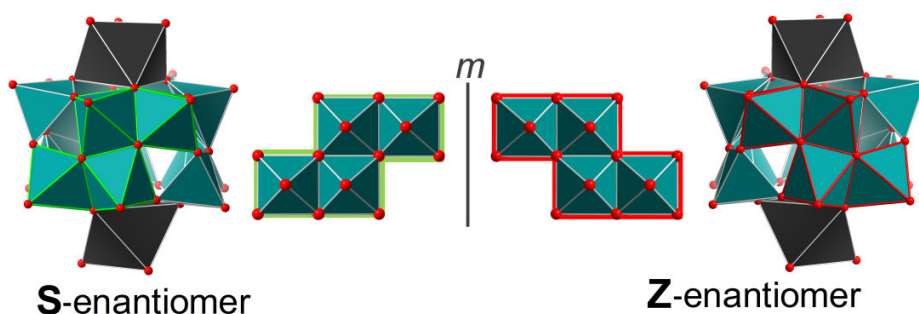


Figure S2. Illustration of the S- and Z- enantiomers observed in the crystal lattice of compound **1**, highlighting the chiral $\{V_4\}$ building units.

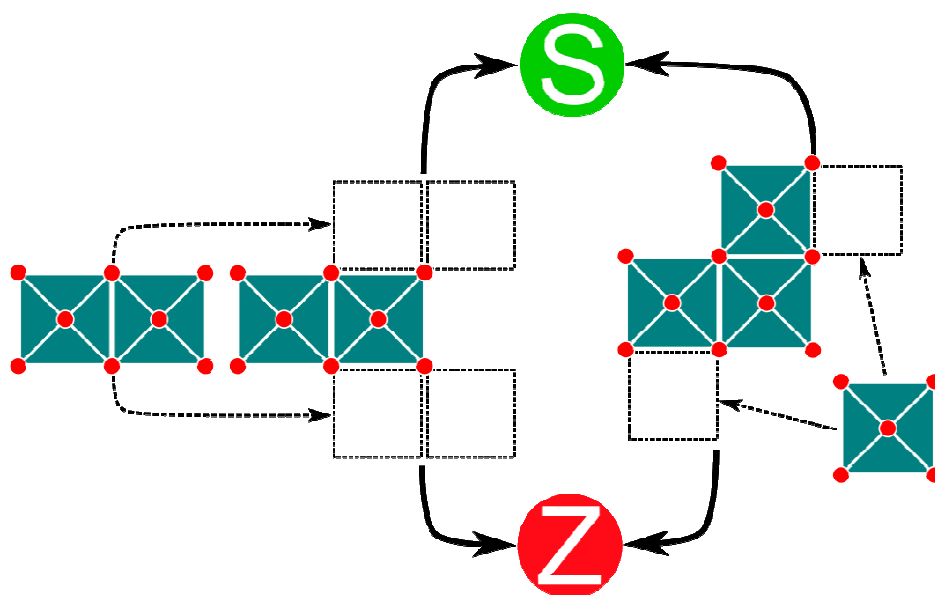


Figure S3. Symmetry breaking leading to the formation of the S- and Z- $\{V_4\}$ building blocks: Left: 2+2 mechanism where two achiral $\{V_2\}$ units are linked to give the chiral S- or Z- $\{V_4\}$ unit. Right: 3+1 mechanism where an achiral $\{V_3\}$ unit is linked with an achiral $\{V_1\}$ unit giving the chiral S- and Z- $\{V_4\}$ units.

Table S2. Bond-valence calculations for compound 1

Atom	BVS	σ , %
Ce1	3.145	5
V1	4.998	0
V2	5.047	1
V3	4.984	0
V4	4.892	2
V5	5.059	1
V6	4.854	3

S4. Cryospray ionization mass-spectroscopy

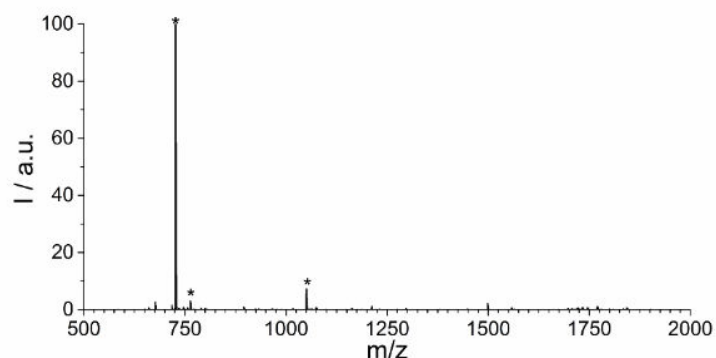


Figure S4. Negative mode CSI-MS spectrum of **1** in DMF, ca. 1×10^{-4} M. Signals labeled with an asterisk (*) were assigned based on m/z and isotopic pattern analysis.

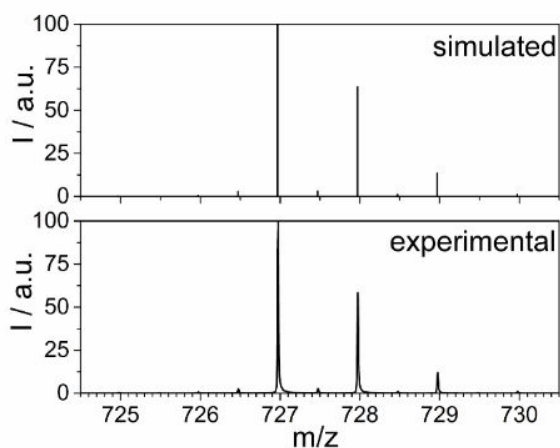


Figure S5. Isotopic pattern peak assignment **1** for m/z 726.98 (calcd. 726.97) represents the cluster core of compound **1**: $[\text{Ce}_2\text{V}_{12}\text{O}_{33}\text{Cl}]^{2-}$. Signals indicate ligand exchange during the CSI experiment.

Table S3. CSI-MS peak assignment for **1**

Rel. Intensity, %	m/z , measured	m/z , simulated	Assigned fragment
100	726.98	726.97	$[\text{Ce}_2\text{V}_{12}\text{O}_{33}\text{Cl}]^{2-}$
3	763.50	763.50	$[\text{Ce}_2\text{V}_{12}\text{O}_{33}\text{Cl}(\text{dmf})]^{2-}$
7	1050.72	1050.72	$[(\text{Ce}_2\text{V}_{12}\text{O}_{33}\text{Cl})_2(\text{C}_{16}\text{H}_{36}\text{N})]^{3-}$

S5. Thermogravimetric analysis

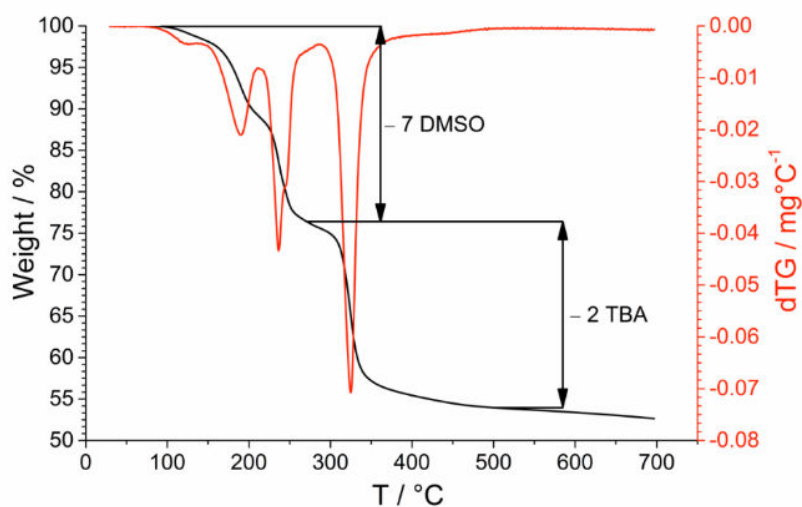


Figure S6. TGA and DTG for **1** showing loss of 7 DMSO molecules (23.85 % (calcd. 26.52%), 20 – 272 °C) and loss of 2 $n\text{Bu}_4\text{N}^+$ cations (22.40% (calcd. 23.50%), 272 - 510 °C).

S6. UV-Vis-NIR spectroscopy

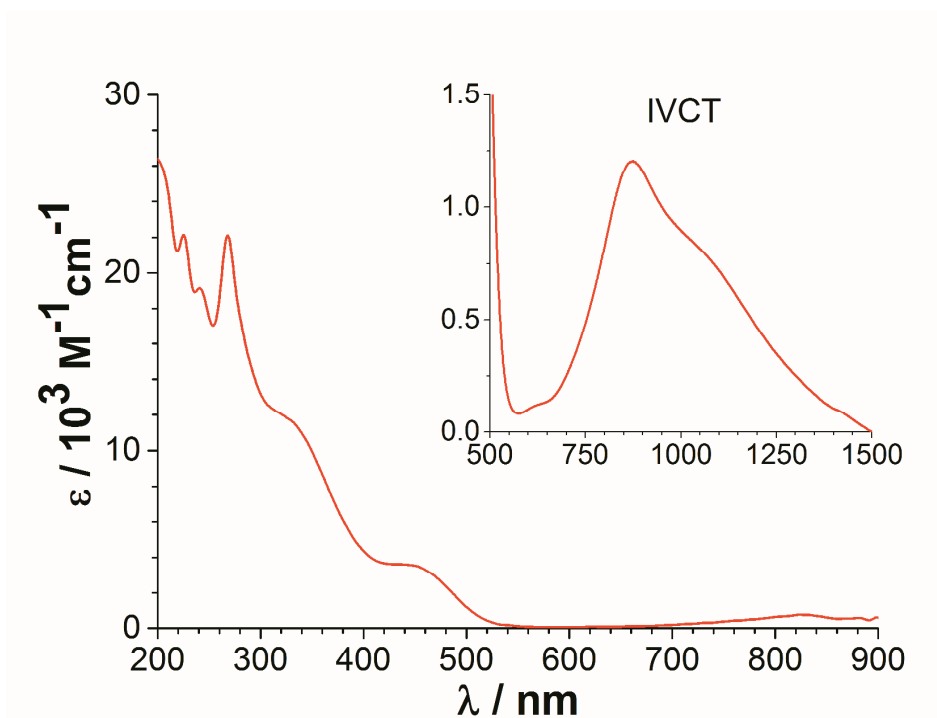


Figure S7. UV-Vis-NIR spectrum for compounds **1** recorded in DMF under ambient conditions.

S7. Photooxidative activity

Photocatalytic activity was tested using the photooxidative decomposition of indigo in homogeneous DMF solution as a benchmark reaction. The reaction was performed at molar ratio of [Cluster] / [Ind] = 1 / 5. [Cluster]₀ = 0.60 mM, [Ind]₀ = 3.00 mM. UV-Vis spectrometry was used to trace the kinetics of the photoreaction as the systems were irradiated with InGaN LEDs, $\lambda_{max} = 405$ nm ($P_{nominal} \sim 20$ W). Due to O→V LMCT bands in the visible, the clusters are capable of light absorption at the given wavelength, promoting irreversible dye decomposing. Additionally it has been proven than cerium(III) chloride does not show photooxidative activity under identical reaction conditions. Observed rate constants k_{obs} was determined by linear regression of the data using zeroth-order kinetics, $k_{0,obs} = 3.62 \times 10^{-5}$ mol L⁻¹ min⁻¹.

Quantum efficiency was determined using a custom-built system reported by Riedle and König.^{S6}

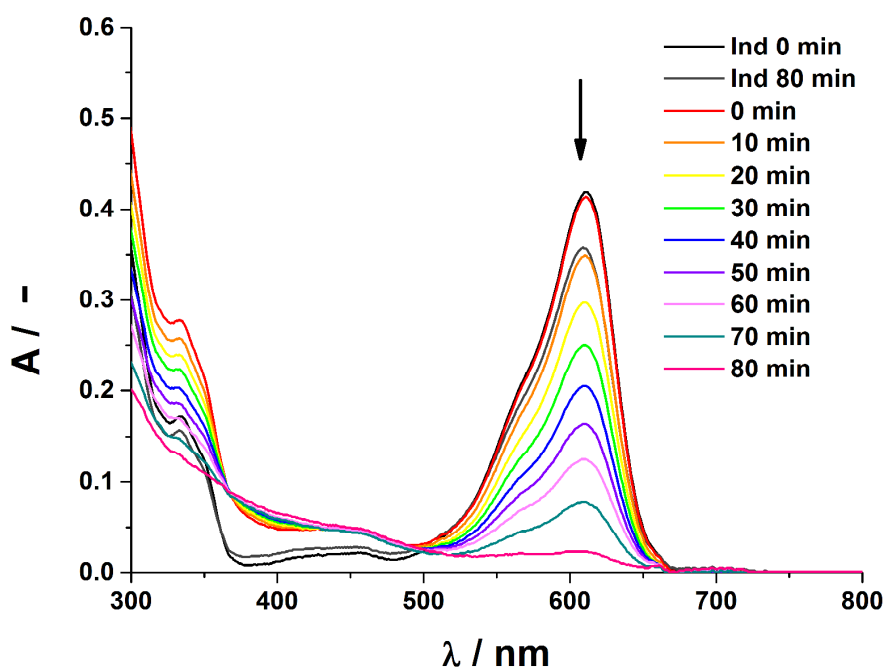


Figure S8. Indigo photooxidation by **1** in DMF, [Cluster] : [Ind] = 1 : 5, irradiated at $\lambda_{max} = 405$ nm.

In order to demonstrate recyclability and stability of **1**, three consecutive runs using the same sample of **1** were performed (conditions: [1] = 3 mM, [1] / [Ind] = 1 / 1). After dye decomposition cycle additional aliquots of indigo were added and the system was irradiated under identical experimental conditions. As shown on Figure S9, virtually identical photooxidative activity is observed. for Run 1 - 3.

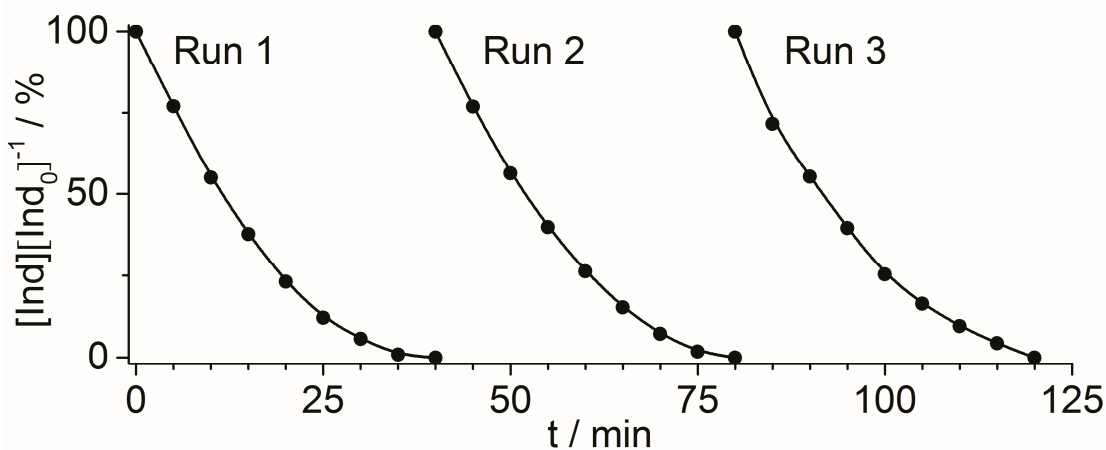


Figure S9. Recyclability of **1** shown by three consecutive indigo photooxidation runs.

Cluster stability was further investigated by UV-Vis spectroscopy. Comparison of the cluster sample before Run 1 (black line) and after Run 1, 2 and 3 show that in the UV-Vis region, no significant changes (apart from signal decrease due to indigo degradation) are observed, showing that **1** is structurally stable under turnover conditions. This is further supported by analysis of Runs 1-3 where only marginal changes in the degradation kinetics are observed (see Fig. S9).

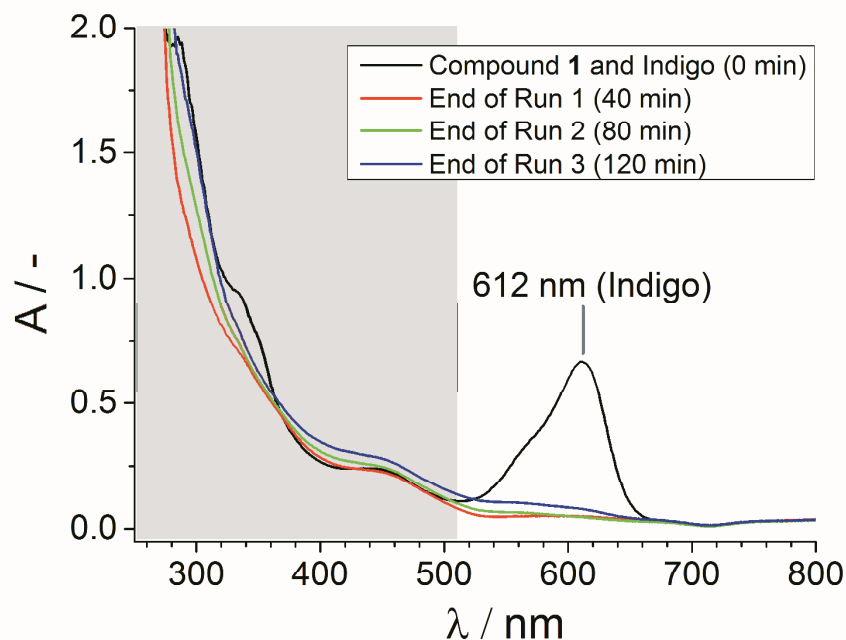


Figure 10. UV-Vis spectra of the reaction mixtures before photocatalytic indigo degradation (black) after Run 1 (orange), Run 2 (green) and Run 3 (blue), showing only minor changes to the characteristic UV-VIS absorption signals of compound **1**. Spectra were recorded in DMF under typical photocatalytic conditions (described above).

Comparative photooxidative activity studies were carried out at three irradiation wavelengths to compare the reactivity of **1**, $(n\text{BuN})_3[\text{H}_3\text{V}_{10}\text{O}_{28}]$ and $(n\text{BuN})_4[\text{V}_4\text{O}_{12}]$, all employed at identical molar concentrations under identical experimental conditions. It can be seen that at 405 nm irradiation, $[\text{H}_3\text{V}_{10}\text{O}_{28}]^{3-}$ features the best dye degradation kinetics whereas at 450 nm and 505 nm, **1** and $[\text{H}_3\text{V}_{10}\text{O}_{28}]^{3-}$ are in a similar range and $[\text{V}_4\text{O}_{12}]^{4-}$ shows only limited activity.

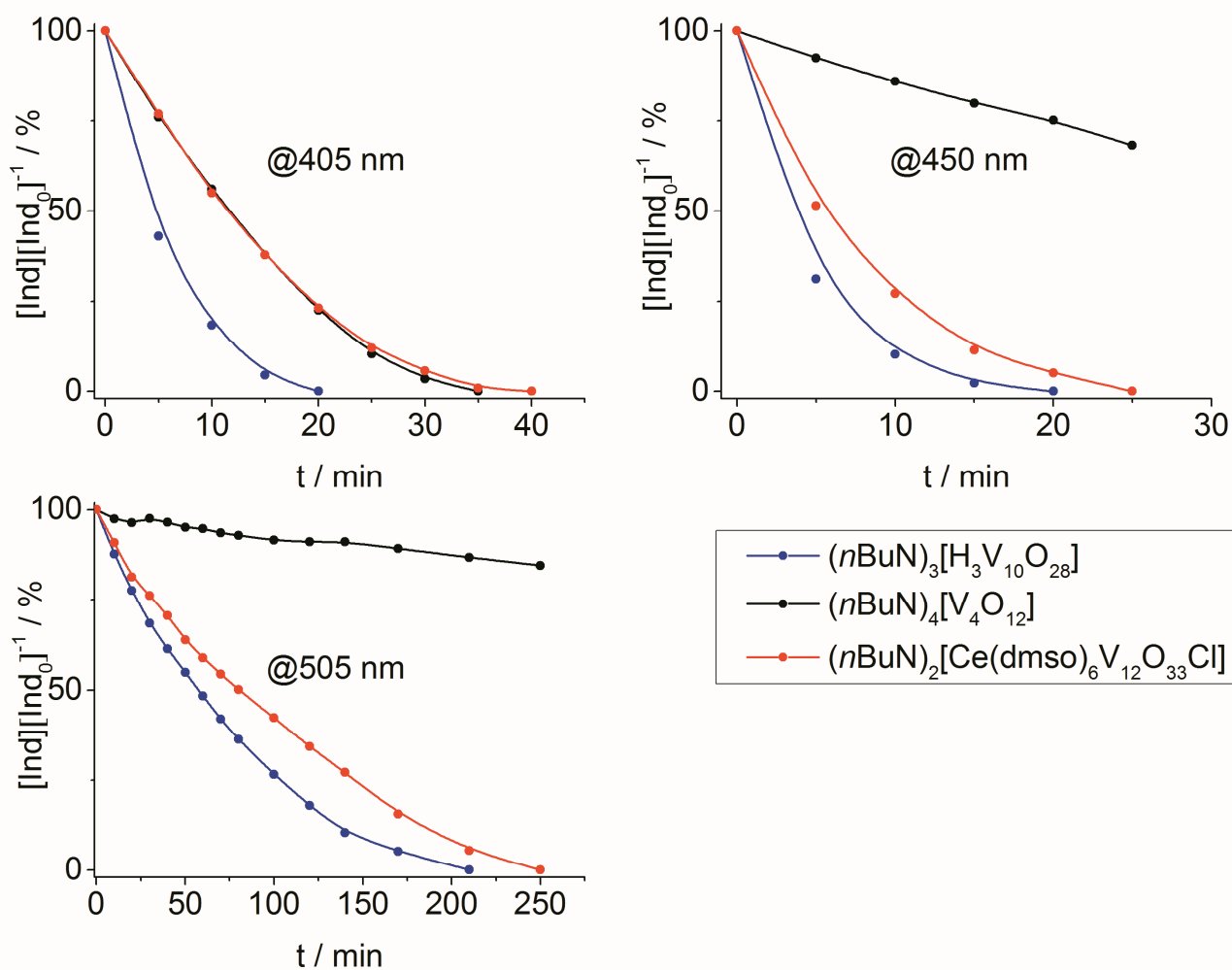


Figure S11. Comparison of the photocatalytic activity for **1**, $(n\text{BuN})_3[\text{H}_3\text{V}_{10}\text{O}_{28}]$ and $(n\text{BuN})_4[\text{V}_4\text{O}_{12}]$ depending on the irradiation wavelength

Further, the photooxidative activity of **1** was evaluated under aerated and deaerated conditions and it was found that in the absence of oxygen, cluster reactivity is significantly reduced, suggesting that cluster reoxidation is dependent on the presence of oxygen. Experimental setup: The cuvette was bubbled with argon for approx. 10 min to eliminate traces of oxygen and nitrogen. The cell remained sealed during irradiation.

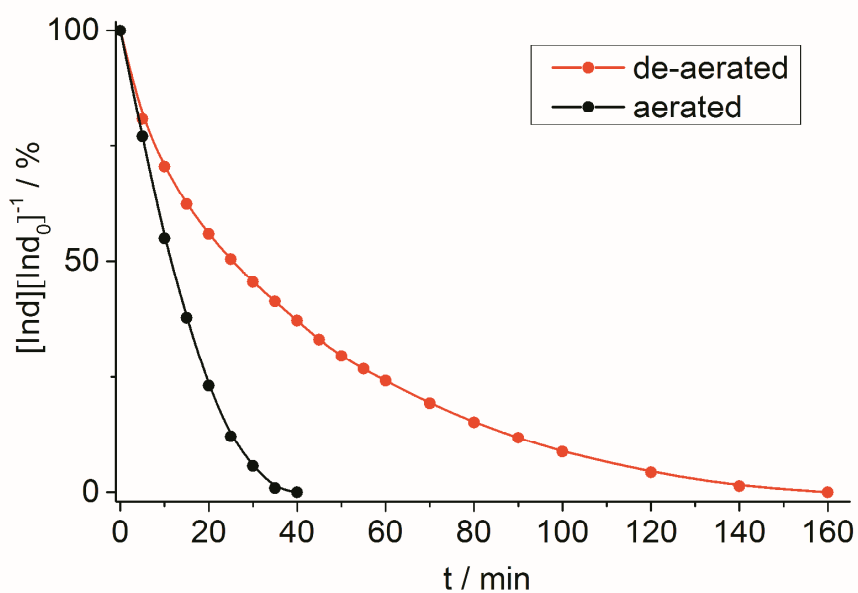


Figure S12. Kinetics measured under anaerobic conditions suggests the significant reduction of the reaction constant

To evaluate the formation of hydroxyl radicals upon irradiation, an excess of hydroxyl scavenger (here: ethanol) was added to the standard indigo oxidation reaction. However, no significant change of reactivity was observed, strongly suggesting that the indigo photooxidation is not dependent upon hydroxyl radicals. Experimental conditions: aliquots of ethanol (approx. 25-fold and 50-fold excess based on $[\text{Ind}]_0$) were added to the standard reaction setup.

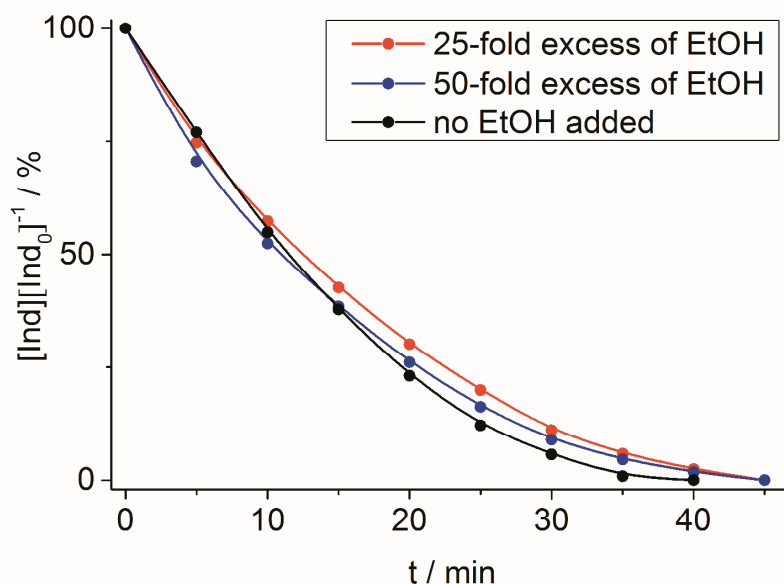


Figure S13. Addition of ethanol as hydroxyl scavenger does not show any significant influence on indigo decomposition. Standard photocatalytic conditions were employed (see above).

S8. Bibliography

- S1. S. Nakamura and T. Ozeki, *J. Chem. Soc. Dalton Trans.*, 2001, 472–480.
- S2. J. Forster, B. Rösner, M. M. Khusniyarov, and C. Streb, *Chem. Commun.*, 2011, **47**, 3114.
- S3. G. M. Sheldrick, *Acta Crystallogr. A*, 2007, **64**, 112–122.
- S4. O. V. Dolomanov, L. J. Bourhis, R. J. Gildea, J. A. K. Howard, and H. Puschmann, *J. Appl. Crystallogr.*, 2009, **42**, 339–341.
- S5. A. L. Spek, *Acta Crystallogr. D Biol. Crystallogr.*, 2009, **65**, 148–155.
- S6. U. Megerle, R. Lechner, B. König, and E. Riedle, *Photochem. Photobiol. Sci.*, 2010, **9**, 1400.